

Electronic Supplementary Information

Controllable porous membrane actuator by gradient infiltration of conducting polymers

Ju Eun Yim^{a,1}, Seung Heon Lee^{a,1}, Seongpil Jeong^{a,b}, Kai A. I. Zhang^c, Jeehye Byun^{a,b}*

^aWater Cycle Research Center, Korea Institute of Science and Technology (KIST), Republic of Korea

^bDivision of Energy & Environment Technology, KIST School, University of Science and Technology, Republic of Korea

^cDepartment of Materials Science, Fudan University, Shanghai 200433, P.R. China

¹Equal contribution.

Materials: Iron(III) chloride hexahydrate, 3,4-ethylenedioxythiophene, acetonitrile, dimethyl formaldehyde, tetrahydrofuran, dimethylsulfoxide, 2-propanol and 1, 4-dioxane were obtained from Sigma Aldrich. Acetone, ethyl alcohol, methyl alcohol, dichloromethane, chloroform, ethyl acetate, n-hexane and ether were purchased from Samchun Korea. Hydrophobic and hydrophilic PVDF commercial membranes (0.45 μm pore size) from Merck Millipore, fluorodyne membrane (0.45 μm pore size) from Pall Corporation, nylon membrane (0.2 μm pore size) from CHMLAB, and polycarbonate membrane (0.4 μm pore size) from Whatman™ were supplied. Pyrrole and 3-hexylthiophene were purchased from TCI Korea. All the chemicals and solvents were used without purification otherwise noted. Water was used in Millipore quality (< 18.2 M Ω cm).

Characterization: Field emission-scanning electron microscope (FE-SEM) was utilized to analyze the surface morphology and the thickness of membrane samples by using a Hitachi Regulus 8230 and an Inspect F. The SEM-Energy-dispersive X-ray (EDX) analysis was performed to determine the infiltration coating depth with conducting polymers. X-ray photoelectron spectroscopy (XPS) data was obtained with Thermo Fisher Scientific Nexsa equipped with a microfocus monochromatic Al-K α source. Beam spot size was 400 μm x 400 μm and a dual neutralizer (Argon ion + electrons) was used. The obtained XPS spectra were fitted using CasaXPS, where the C(1s) line for adventitious carbon was found at 284.8 eV. Infrared thermographic imaging was done with a Seek Thermal ShotPro Infrared Camera. X-ray diffraction (XRD) pattern of samples was acquired by using a Rigaku Dmax2500/PC. Fourier-transform infrared spectroscopy (FT-IR) measurement was conducted with a Thermo scientific NICOLET iS10 with a KBr/Ge mid-infrared beam splitter. Solvent uptake was estimated gravimetrically, where a 1.5 cm x 0.5 cm membrane sample was stored in 1,4-dioxane (10 mL) for 1 h and weighed carefully. The sample was dried in a vacuum oven for 1 h and the weight was reevaluated. Solvent uptake was calculated using the following equation;

$$\text{Solvent uptake (\%)} = \left(\frac{W_w - W_d}{W_d} \right) * 100$$

where W_w and W_d are the weights of the wet and dry membrane samples, respectively.

Preparation of porous membrane actuator: In order to make the membrane actuator with polypyrrole (PPy) infiltration coatings, PVDF membrane (typically 1.5 cm X 4 cm size) was added by 0.1 mL of 30 wt% iron(III) chloride solution (in ethanol) and dried for 3 min under air. The membrane was then placed in a glass chamber (\varnothing 95 mm), where 20 μl of pyrrole monomer was charged next to the membrane. The polymerization time varied 3, 10, 30, 60, and 120 min to investigate the effect of infiltration coating depth for actuation. After the vapor phase polymerization (VPP) of pyrrole, the coated membrane was intensively washed with methanol to remove the unreacted oxidant and monomer. The coated membrane was dried under air for further use, giving the PVDF/PPy membrane actuators. A large-scale PVDF/PPy actuator (7 cm X 12 cm) was made by using 1.2 mL of 30 wt% FeCl $_3$ solution (4 min for dry) and 250 μl of pyrrole monomer in the bigger glass chamber (\varnothing 140 mm). For the synthesis of PVDF/PEDOT and PVDF/P3HT, 3,4-ethylenedioxythiophene(EDOT) and 3-hexylthiophene(3HT) were polymerized using the same method described above, except the

polymerization temperature was kept to be 80°C for 5 min (PEDOT) and 20 min (P3HT), respectively.

For surface patterning on the membrane actuator, liquid masking and tape masking methods were utilized. The liquid masking was done by means of the hydrophobic nature of commercial PVDF membrane, in which water droplet on the membrane acts as a mask which prevents pyrrole vapor from reacting with oxidants. Since iron(III) chloride is very soluble in water, longer VPP time might lead to the dissolution of oxidant into the water droplet and further the polymerization of pyrrole in the droplet. The VPP time for the liquid masking was thus optimized to be 10 min. Tape masking is a facile method to make various patterns on the PVDF membrane with 3M Scotch tape (12 mm). To prevent very reactive pyrrole vapor from diffusing through the tape layer, we used 3 layers of tape, freshly cut and attached to the oxidant-coated PVDF membrane. The maximum VPP time for tape masking was 30 min due to the unwanted polymerization at the edge of tape boundary when over 30 min. After the polymerization, the tape mask can be easily removed during washing the membrane in methanol. For the best performing actuator with the tape masking, the polymerization was repeated twice for total 60 min of VPP time.

Characterization of mechanical property: The surface mechanical properties of pristine PVDF and PVDF/PPy actuators were measured by nano-indentation test using Bruker TI-950 with a Berkovich tip. The nano-indentation experiment was conducted in the load-controlled mode where the indentation load was fixed at around 400 μN for all cases. The indentation was applied 10-15 points on each tested membranes. Elastic modulus (E) and hardness (H) were determined from indentation load-displacement data by Oliver and Pharr method^[1]. Hardness can be defined as the mean pressure under the nano-indenter which can be derived from the following equation;

$$H = \frac{P_{max}}{A_C}$$

where P_{max} (μN) is the maximum applied force from the load-displacement curve and A_C (nm^2) is the contact area of the indenter tip on the sample.

The reduced modulus (M_r) was obtained from the initial slope of the unloading curve (dP/dh) which can be formulated as follows;

$$S = \frac{dP}{dh} = \beta \frac{2}{\sqrt{\pi}} M_r \sqrt{A_C}$$

where S is the contact stiffness, P is the applied force to the indenter, h is the displacement, β is a correction factor related to the geometry of indenter, and M_r is the reduced modulus of the nano-indenter.

Finally, the elastic modulus of sample can be obtained by the following equation;

$$\frac{1}{M_r} = \frac{1 - \nu_s^2}{E_s} + \frac{1 - \nu_i^2}{E_i}$$

Where E_s and ν_s are elastic modulus and Poisson's ratio for the sample, respectively. E_i and ν_s are the same parameters for the indenter which are given as 1140 GPa and 0.07, respectively. From the literature, Poisson's ratio for PPy and PVDF was found to be 0.278^[2]

and 0.34^[3], respectively, allowing us to determine the elastic modulus (E_s) of tested membranes.

Characterization of membrane porosity: Pristine PVDF and PVDF/PPy actuators made in different VPP times were analyzed with a capillary flow porometer (CFP-1500AEL, PMI) to measure the pore size distribution and the air permeability. Wet/dry flow method was utilized to characterize the membrane pore diameter and dry flow method was used to identify the membrane permeability at different pressure range. Galwick fluid (surface tension 15.9 mN m⁻¹) was employed as the wetting liquid for the complete wetting of tested membranes.

Solvent vapor stimulus actuation: The PVDF/PPy membrane actuator was cut into the size of 1.5 cm X 4 cm. All solvents used for actuation test had a volume of 90 mL in a 250 mL glass beaker. The membrane actuators were brought inside the solvent beaker and the vapor stimulus actuation was recorded above the liquid surface. Bending angle by the actuation was calculated at the maximum bending point of membrane actuator. Response time was defined as the time taken from the point where the sample enters the beaker to its maximum bending point. The recovery time was defined as the time taken from its maximum bending point to its original shape outside of the solvent beaker. Reversible actuation performance was tested by recording 100 repeated cycles of vapor stimulus actuation in acetone (30.6 kPa, 25 °C). Between the cycles, the membrane actuator was blown with dry air to completely desorb acetone vapor molecules.

In-solvent stimulus actuation: The solvent volume was 10 ml and all solvents were used without purification or dilution. Among the tested solvents, 1,4-dioxane with high toxicity was chosen for the in-solvent actuation with different concentration in water, where the concentration of 1,4-dioxane was controlled to be 100, 80, 60, 50, 40, 30, 20, and 10%. The instant bending of the membrane actuator in solvents allows us to lift up the object by wrapping the actuator around the object. Both small (1.5 cm X 4 cm) and large-scale (7 cm X 12 cm) actuators were tested for grasping an object in the solvent to find the maximum weight for lifting.

Solvent leakage detection using an electrical circuit with PVDF/PPy: An electronic circuit was fabricated using a power supply (5 V), a LED bulb, a resistor (10K Ohm) and a PVDF/PPy60 membrane actuator (1.5 cm X 4 cm). The membrane actuator was placed on the tissue paper with a polypropylene (PP) mesh as a spacer to prevent the direct wetting of the membrane. When solvent leaks, the tissue paper is wet and the solvent vapor through the PP mesh actuates the PVDF/PPy, touching a Cu electrode to connect the circuit and light up the LED.

Fig. S1. FT-IR spectra of PVDF and PVDF/PPy.

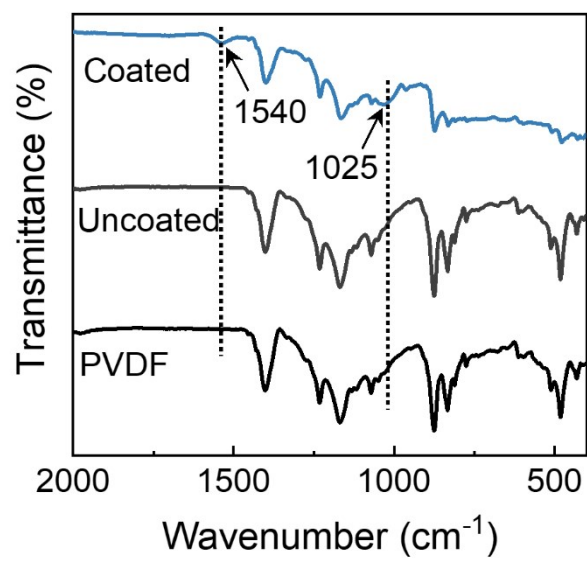
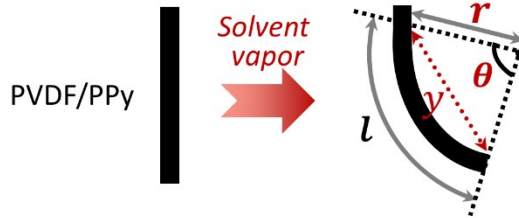


Fig. S2. Bending curvature calculation of PVDF/PPy actuators. l is the length of actuator, r is radius of the bending arc, θ is the bending angle, and y is the chord of bending arc. The length y was measured in optical photographs of bent PVDF/PPy and the bending angle θ was then obtained by equation (2). After deriving the r by equation (1), curvature can be calculated by equation (3).



$$(1) \quad l = r\theta, r = \frac{l}{\theta}$$

$$(2) \quad y = 2r \sin \frac{\theta}{2} = \frac{2l}{\theta} \sin \frac{\theta}{2}$$

$$(3) \quad \text{Curvature} = 1/r$$

Fig. S3. Actuation performance of common porous membranes by infiltration coating of PPy via VPP process. The tested membranes did not respond to acetone vapor before the VPP and became responsive to acetone vapor after the VPP.

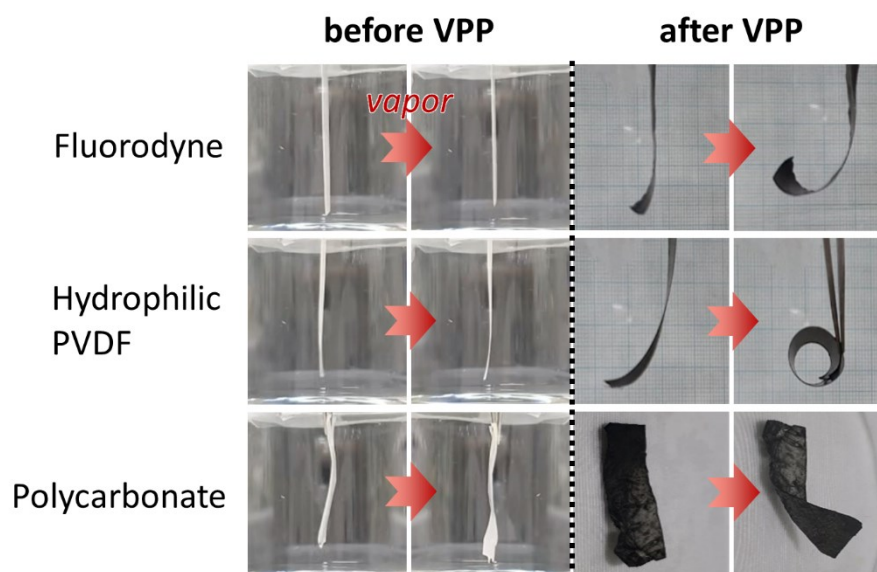


Fig. S4. (a) Pore size analysis by ImageJ software. Scale bar = 5 μm . Original SEM images were converted into black/white binary images where the pores were filled in black. The pore size was counted by a function of 'Analyze particles' in ImageJ, in which the Feret's diameter was used to define the surface pore size. The feret's diameter means the longest distance between two points on the boundary of the given pore. (b) Pore size distribution and (c) mean surface pore size of PVDF and PVDF/PPy. The error bars were obtained from the standard deviation of triplicate measurements.

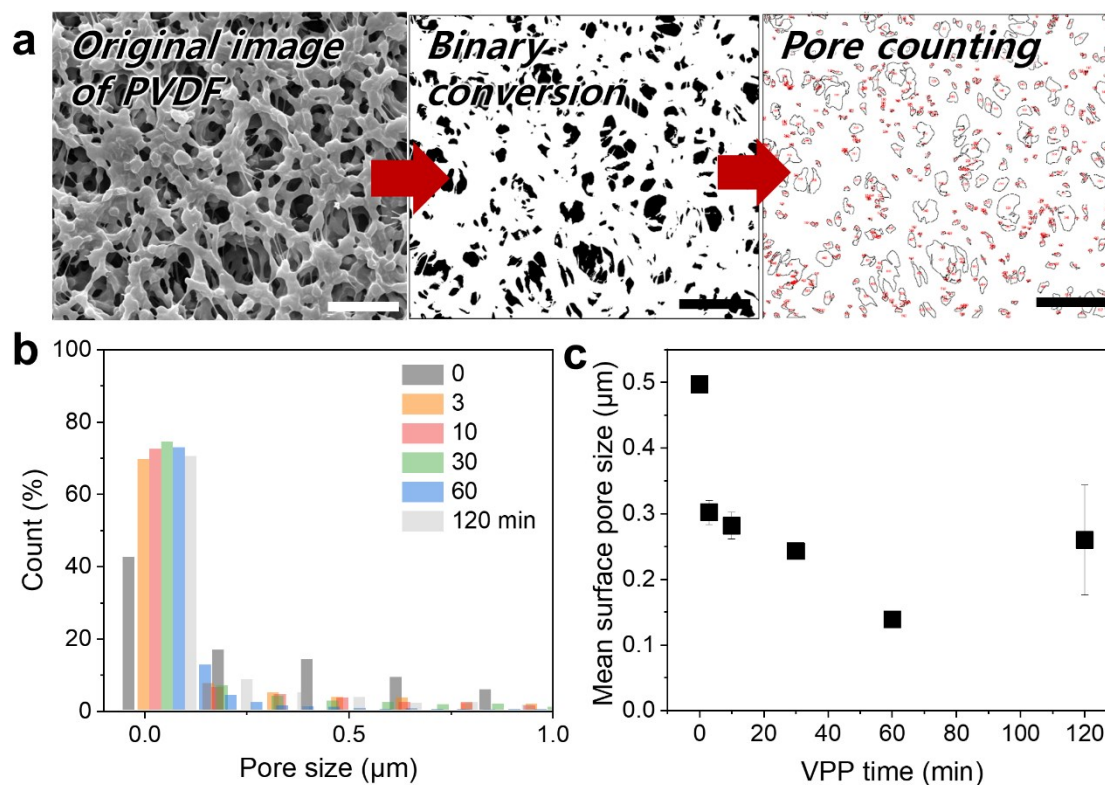


Fig. S5. Back-side SEM images of (a) pristine PVDF, (b) PVDF/PPy3, (c) PVDF/PPy10, (d) PVDF/PPy30, (e) PVDF/PPy60, and (f) PVDF/PPy120. Scale bar = 10 μ m.

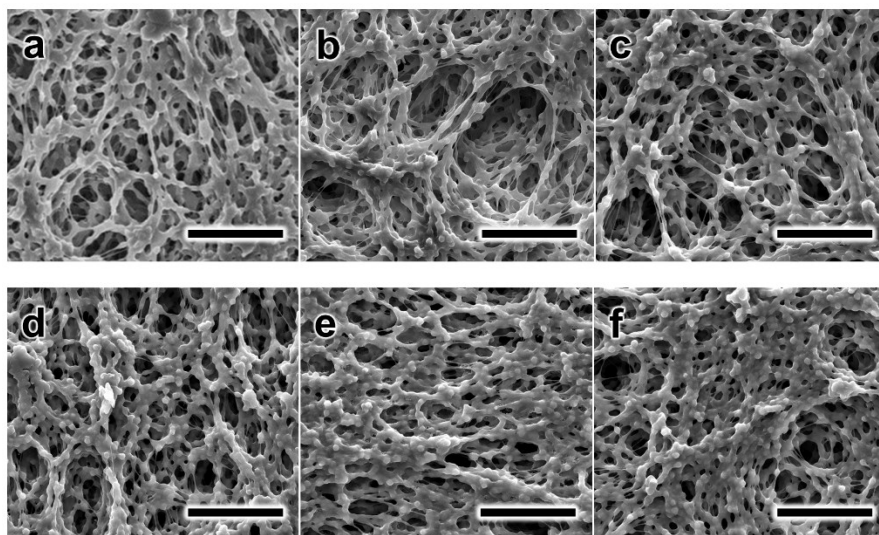


Fig. S6. Cross-section SEM images of (a) pristine PVDF, (b) PVDF/PPy3, (c) PVDF/PPy10, (d) PVDF/PPy30, (e) PVDF/PPy60, and (f) PVDF/PPy120. Scale bar = 50 μm . (g) Thickness of PVDF and PVDF/PPy.

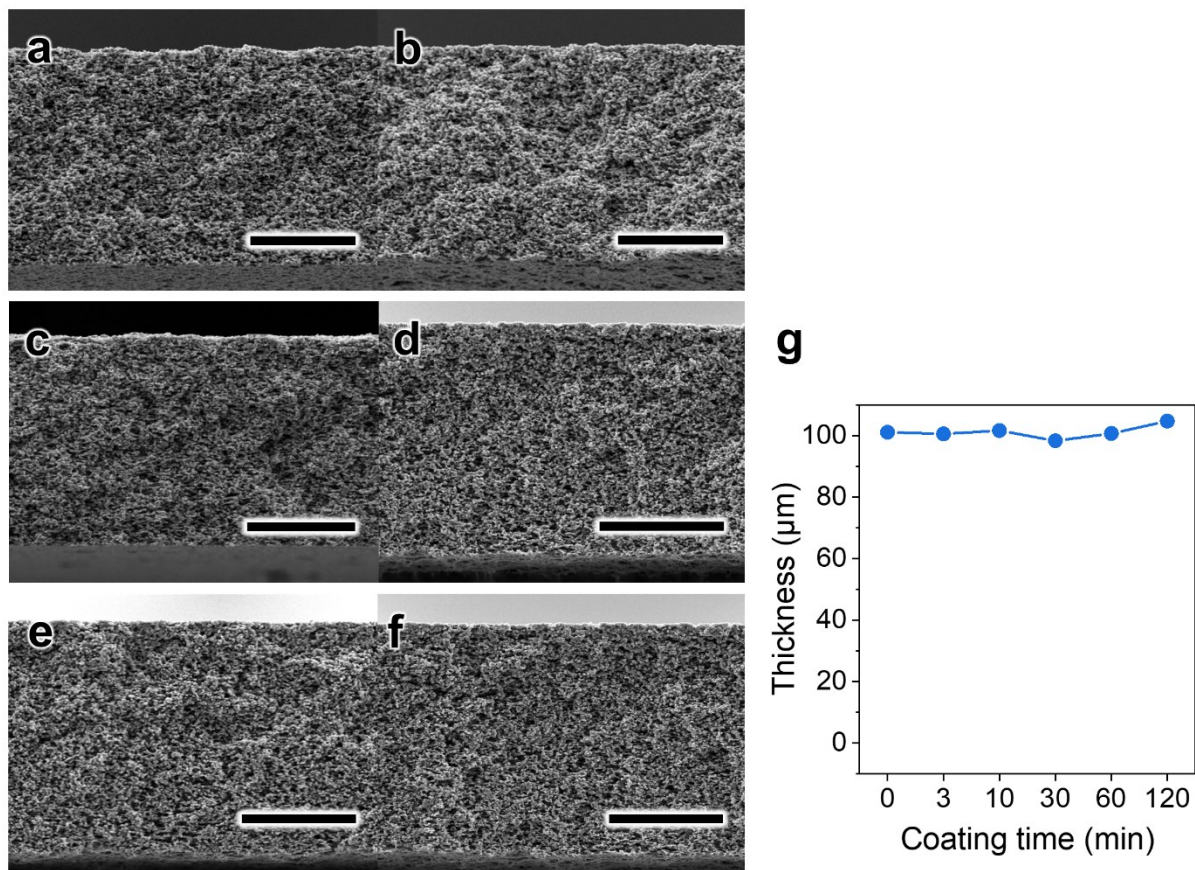


Fig. S7. (a) Cross-section SEM image of PVDF/PPy60 which divided into five areas from top to bottom, A1 to A5. Scale = 50 μm . (b) EDX analysis of the given areas of A1-A5. The nitrogen contents shown in Fig. 2d are the average value of three individual membrane samples, as listed in Table S1.

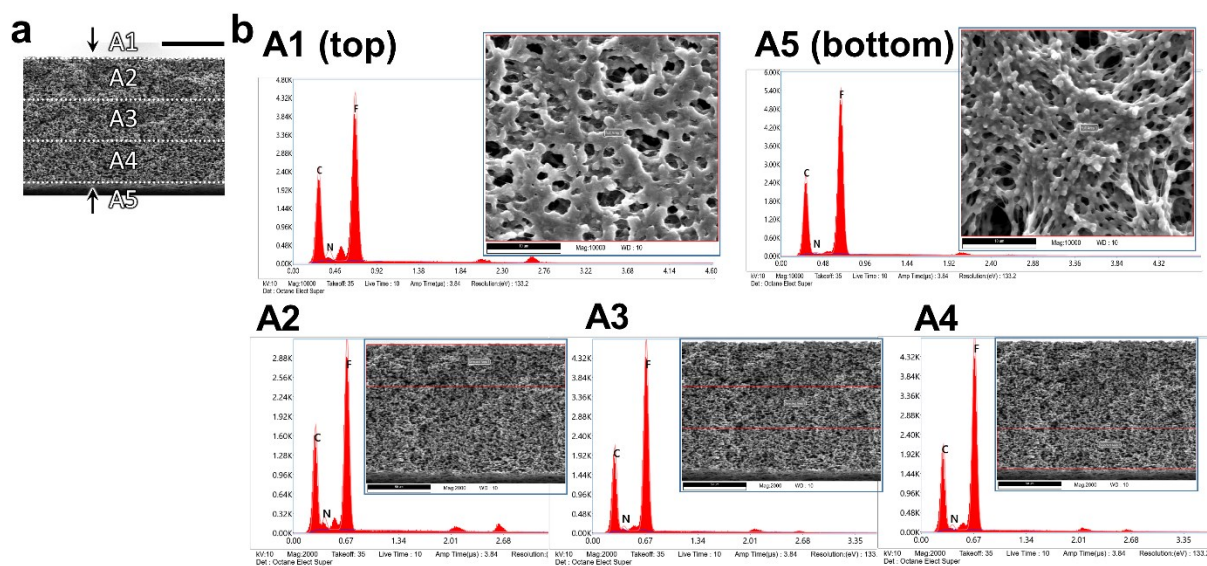


Fig. S8. (a) FeCl_3 -coated PVDF membranes having macroscopic patterns on the surface. Actuation performances of PVDF/PPy30 by the pattern orientation of 0° , 45° , and 90° , at (b) side view, (c) front view, and (d) top view.

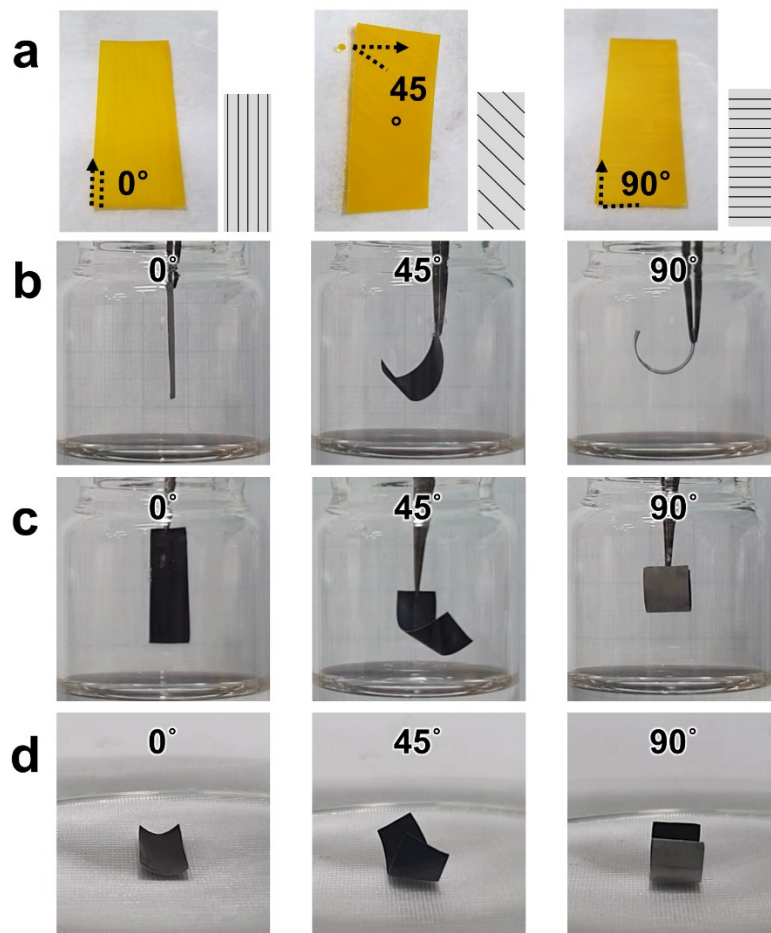


Fig. S9. (a) Optical photographs of PVDF/PPy60 in smaller dimensions under acetone vapor and (b) their actuation performance. **1:** 45 mm x 2 mm, **2:** 40 mm x 2 mm, **3:** 30 mm x 2 mm, **4:** 20 x 2 mm.

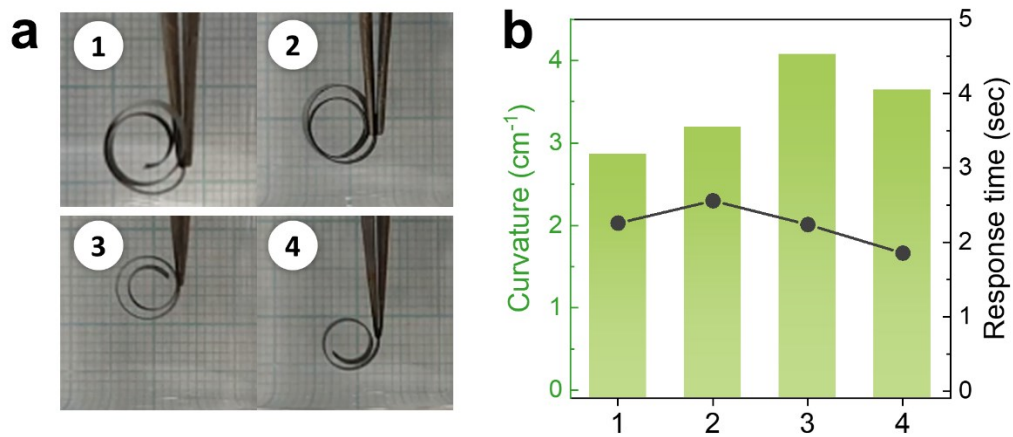


Fig. S10. Actuation performance of PVDF/PPy60 under various solvent vapors.

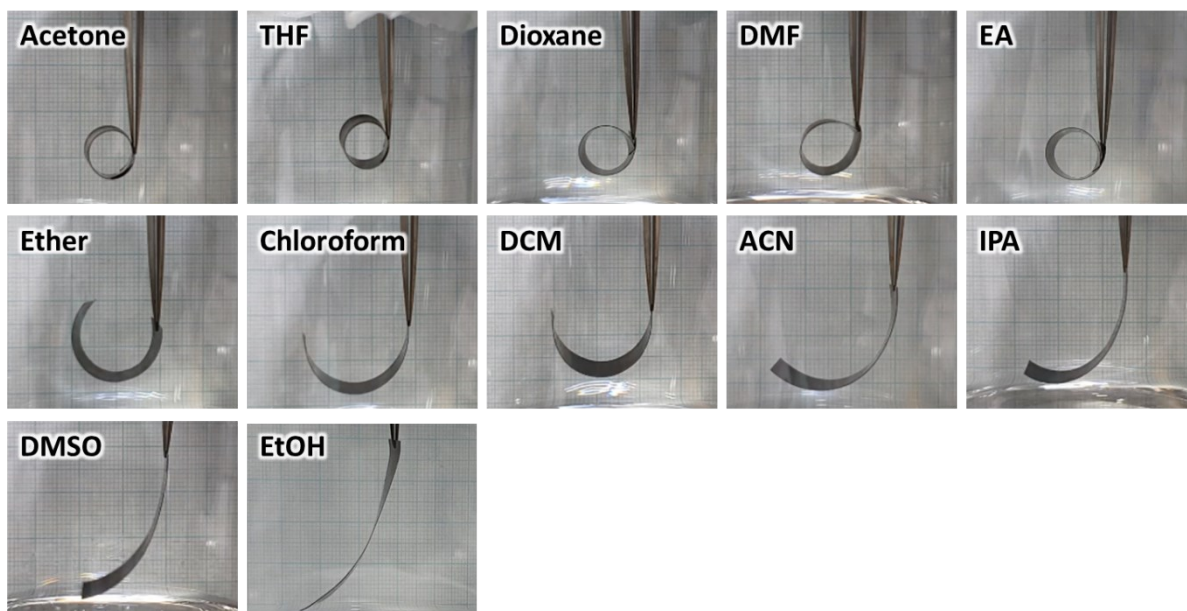


Fig. 11. Actuation performance of PVDF/PPy60 with respect to acetone concentrations in water.

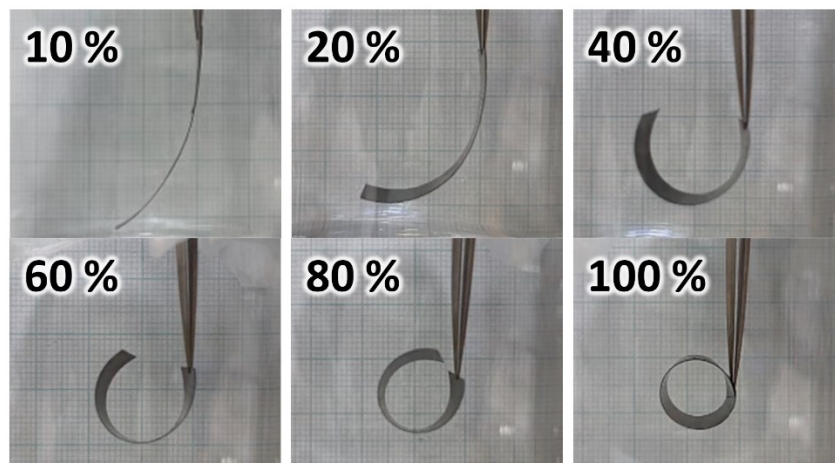


Fig. S12. In-solvent actuation behavior of PVDF and PVDF/PPy immersed in 1,4-dioxane. The size of actuators was 15 mm x 5 mm.

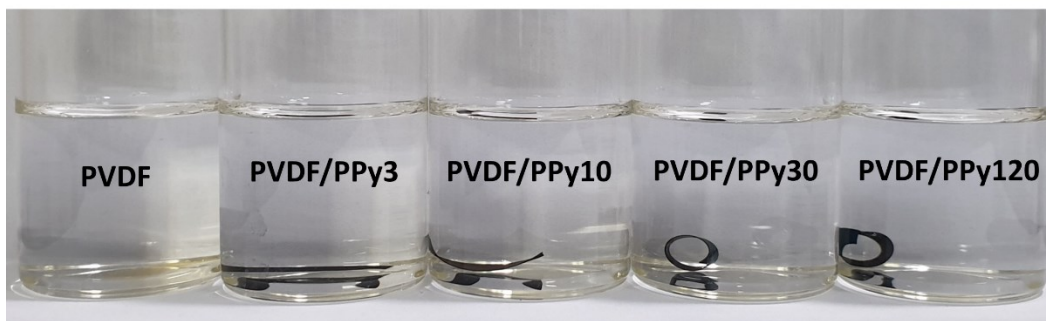


Fig. S13. Actuation performance of PVDF/PPy60 in various solvents. The size of actuators was 4 cm x 1.5 cm.

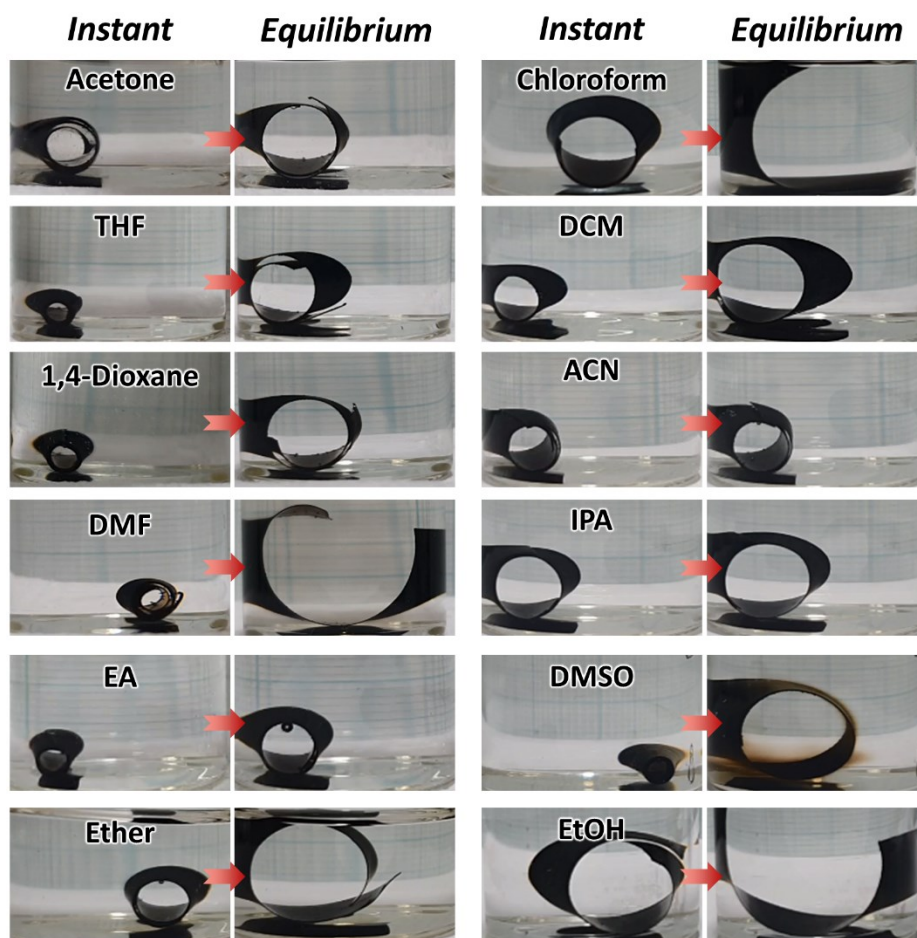


Fig. S14. (a) FT-IR spectra of front and back side of commercial PVDF. Peaks were assigned from reference^[4]. (b) XRD patterns of front and back side of PVDF. The two peaks on XRD pattern indicate α + γ phase of PVDF in planes (110) and (020)^[4].

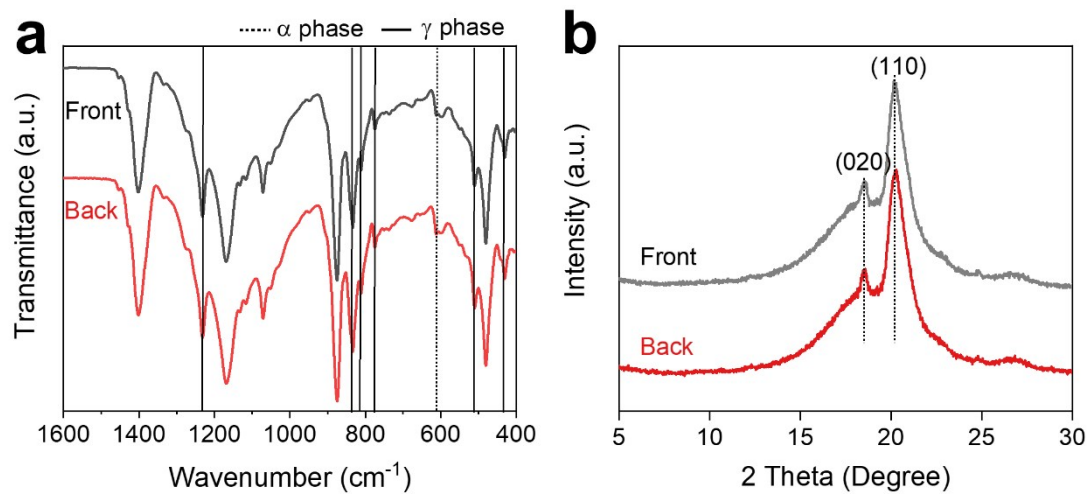


Fig. S15. Change of bending angle when PVDF was coated by PPy one-side and both-sides of membrane for 10 min.

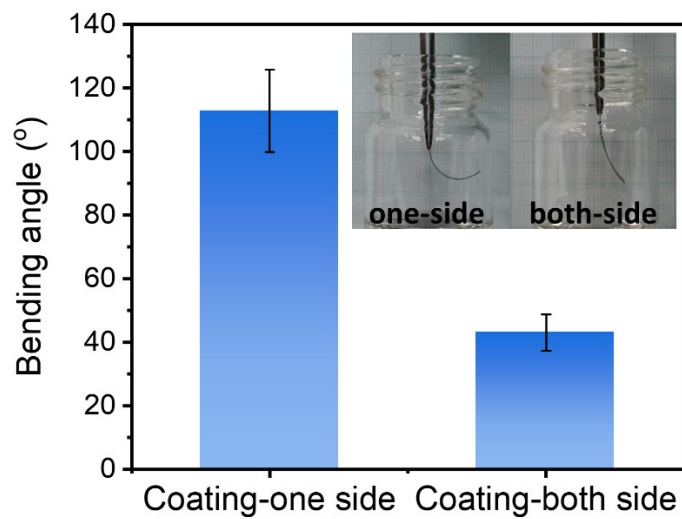


Fig. S16. Surface SEM image and the corresponding EDX analysis of the large-scale PVDF/PPy60 (a) before and (b) after the actuation tests in solvents.

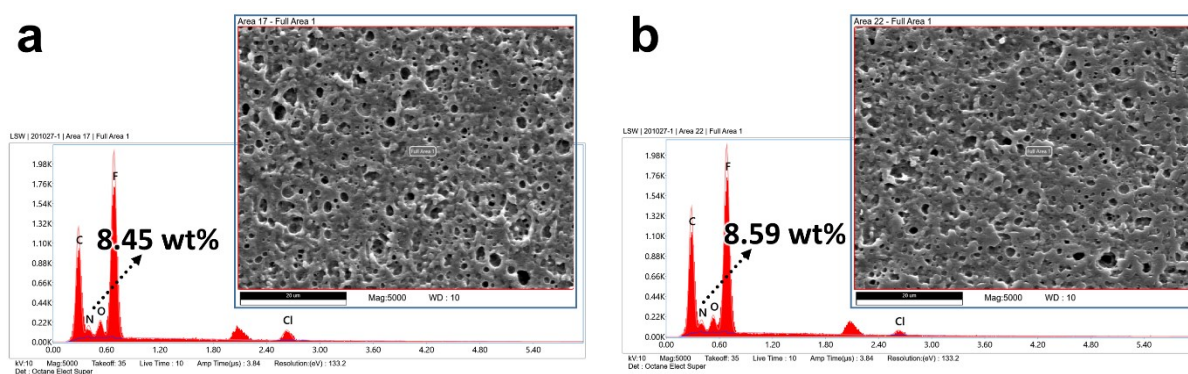


Table S1. Nitrogen contents across the cross-section of PVDF/PPy obtained by SEM-EDX analysis. The average value of each area was displayed in Fig. 2d.

N(wt%)	PVDF-1	PVDF-2	PVDF-3			Average	STD	$\Delta N\%$ (A1-A5)
A1	0	0	0			0	0	0
A2	0	0	0			0	0	
A3	0	0	0			0	0	
A4	0	0	0			0	0	
A5	0	0	0			0	0	
3min	3-1	3-2	3-3	3-4	3-5			
A1	2.24	2.26	2.87	2.95	3.06	2.68	0.39	1.84
A2	0.74	0.97	1.26			0.99	0.26	
A3	0	0	0.6			0.20	0.35	
A4	0.82	0.85	0.89			0.85	0.04	
A5	1.04	0.78	0.69			0.84	0.18	
10min	10-1	10-2	10-3					
A1	3.25	3.34	3.73			3.44	0.26	2.60
A2	3.05	3.41	2.72			3.06	0.35	
A3	1.23	0.94	0.89			1.02	0.18	
A4	0.92	0.94	0.92			0.93	0.01	
A5	0.66	0.84	1.03			0.84	0.19	
30min	30-1	30-2	30-3	30-4				
A1	4.32	4.73	4.91			4.65	0.30	3.55
A2	5.72	3.82	4.45	4.28		4.57	0.81	
A3	1.57	1.38	0.83	1.06		1.21	0.33	
A4	1.68	1.42	1.19	1.22		1.38	0.23	
A5	0.95	1.02	1.34			1.10	0.21	
60min	60-1	60-2	60-3	60-4	60-5			
A1	7.39	9.55	11.26	9.99		9.55	1.61	7.46
A2	8.97	5.11	5.7	5.87	7.94	6.72	1.65	
A3	2.74	1.34	1.38	2.87	2.95	2.26	0.82	
A4	3.02	1.41	1.6	3.01	4.81	2.77	1.37	
A5	1.8	1.72	2.95	1.88		2.09	0.58	
120min	120-1	120-2	120-3					
A1	9.68	10.68	11.04			10.47	0.70	7.00
A2	10.43	9.57	9.56			9.85	0.50	
A3	4.4	4.78	3.69			4.29	0.55	
A4	4.84	7.03	5.03			5.63	1.21	
A5	4.32	3.2	2.87			3.46	0.76	

Table S2. Comparison of actuation performance of polymeric and polymer/carbon hybrid actuators.

Materials	Dimension	Solvent	Curvature	Curvature ×Thickness	Time	Reference
PVDF/PPy60	40 mm × 15 mm × ~100 μm	Acetone	1.74 cm ⁻¹	0.0174	3.1 s	This work
	30 mm × 2 mm × ~100 μm	Acetone	4.07 cm ⁻¹	0.0407	2.2 s	
α-phase PVDF	7 mm × 1 mm × 3 μm	Acetone	32 cm ⁻¹	0.0096	0.4 s	[5]
PS/EVOH nanofibrous film	15 mm × 1 mm × 21 μm	Toluene	21.02 cm ⁻¹	0.0441	0.15 s	[6]
PILf ₂ N/C-pillar[5]arene	20 mm × 1 mm × 30 μm	Acetone	13.3 cm ⁻¹	0.0399	0.4 s	[7]
PIL-PAA@CNTs Membrane	20 mm × 2 mm × 50 μm	Acetone	1.3 mm ⁻¹	0.0650	6 s	[8]
PVA/CNTs@PDMS PVDF layer	20 mm × 10 mm × 50 μm	Acetone	0.65 mm ⁻¹	0.0325	10 s	[9]
Poly _x COF-42 membranes	13 mm × 2 mm × 11 μm	Ethanol	0.62 mm ⁻¹	0.0068	4 s	[10]
GO-PIL/filter paper	20 mm × 1 mm × 107 μm	Acetone	0.53 mm ⁻¹	0.0567	5 s	[11]
Photocrosslinked PVDF@PAM film	3 cm × 0.4 cm × 40 μm	Acetone	0.35 mm ⁻¹	0.0140	1.8 s	[12]
a PCL/PCL-MWCNT film	30 mm × 5 mm × 0.8 mm	CHCl ₃	1.4 cm ⁻¹	0.1120	90 min	[13]
PPy/AG composite films	Rectangular shape (thickness 15.7 μm)	Humidity	1.1 cm ⁻¹	0.0017	2 s	[14]

Supplementary reference

- [1] Y. Hang, G. Liu, K. Huang, W. Jin, *J. Membr. Sci.* **2015**, 494, 205.
- [2] A. Vinogradov, F. Holloway, *Ferroelectrics* **1999**, 226, 169.
- [3] C. Guanggui, D. Jianning, Z. Zhongqiang, L. Zhiyong, P. Huasheng, *Surf. Interface Anal.* **2012**, 44, 844.
- [4] P. Martins, A. C. Lopes, S. Lanceros-Mendez, *Prog. Polym. Sci.* **2014**, 39, 683.
- [5] H. Deng, Y. Dong, C. Zhang, Y. Xie, C. Zhang, J. Lin, *Mater. Horiz.* **2018**, 5, 99.
- [6] Y. Jin, Q. Zhu, W. Zhong, K. Yan, D. Wang, *J. Phys. Chem. C* **2019**, 123, 185.
- [7] Q. Zhao, J. W. C. Dunlop, X. Qiu, F. Huang, Z. Zhang, J. Heyda, J. Dzubiella, M. Antonietti, J. Yuan, *Nat. Commun.* **2014**, 5, 4293.
- [8] H. Lin, J. Gong, M. Eder, R. Schuetz, H. Peng, J. W. C. Dunlop, J. Yuan, *Adv. Mater. Interfaces* **2017**, 4, 1600768.
- [9] X. Su, H. Li, X. Lai, Z. Chen, X. Zeng, *Chem. Eng. J.* **2020**, 394, 124919.
- [10] Z. Wang, Q. Yu, Y. Huang, H. An, Y. Zhao, Y. Feng, X. Li, X. Shi, J. Liang, F. Pan, P. Cheng, Y. Chen, S. Ma, Z. Zhang, *ACS Cent. Sci.* **2019**, 5, 1352.
- [11] H. Song, H. Lin, M. Antonietti, J. Yuan, *Adv. Mater. Interfaces* **2016**, 3, 1500743.
- [12] J. Wei, X. Qiu, L. Zhang, *ACS Appl. Mater. Interfaces* **2019**, 11, 16252.
- [13] A. Toncheva, B. Willocq, F. Khelifa, O. Douheret, P. Lambert, P. Dubois, J.-M. Raquez, *J. Mater. Chem. B* **2017**, 5, 5556.
- [14] T. Wang, M. Li, H. Zhang, Y. Sun, B. Dong, *J. Mater. Chem. C* **2018**, 6, 6416.

Supplementary movie

Movie S1. Actuation performance of PVDF/PPy membranes by VPP time in response to acetone vapor.

Movie S2. Actuation performance of PVDF/PPy membranes by VPP time in response to dioxane solvent.

Movie S3. Biomimetic actuation of liquid-masked PVDF/PPy60 under the acetone vapor like tree leaves.

Movie S4. Biomimetic actuation of tape-masked PVDF/PPy60 under the acetone vapor like flower petals.

Movie S5. Large-scale PVDF/PPy60 mimicking a human hand motion under the exposure to acetone vapor.

Movie S6. PVDF/PPy60 electrical switch for acetone leakage detection.

Movie S7. PVDF/PPy60 soft gripper lifting up a metal paper clip submerged in dioxane.

Movie S8. PVDF/PPy60 soft gripper lifting up a heavy plastic basket submerged in dioxane.